博士論文

Ultrathin Membranes of Artificial Lignin

人工リグニン超薄膜

符　騰飛

Ultrathin Membranes of Artificial Lignin

（人工リグニン超薄膜）

相田研究室 37-177288 符 騰飛(Tengfei FU)

【1】Introduction

Lignin, as one of the most abundant nature polymers, accounts for approximately 30% of the organic carbon on earth and exists in almost all terrestrial plants. The main role of lignin is to confer plants enough mechanical rigidity by enhancing the structure of secondary cell walls. Chemically, lignin is an amorphous three-dimensionally crosslinked polyphenolic polymer, whose rigid aromatic skeleton carries a large amount of phenolic hydroxyl groups[1]. Because of such aromatic network, lignin is both mechanically tough and chemically resistant to degradation. Previously, during the pulping process of paper manufacture, lignin is separated as a waste product from wood and generally burned as a fuel. Recently, many attractive properties of lignin such as antioxidation, UV-shielding, antimicrobial, and antiviral activities[2] were reported and encouraged many researchers to explore lignin-based functional materials for valuable applications. However, one of the serious problems for this direction is the poor processability of lignin. Currently, lignin can be obtained only in a form of a powder and cannot be processed to any other forms without making a composite with other processable polymers, where most of the attractive feature of lignin (mechanical and chemical robustness) would be gone. This fact is a huge drawback for the development of materials based on lignin.

In 2015, Aida group reported how a salt bridge can be reinforced by a hydrophobic interface nearby in a sub-nanometer regime using a self-assembled monolayer on silicon water electrode[3]. In this work, the authors provided a new method to generate a pH gradient on the electrode surface and utilized it for protonation/deprotonation of the salt bridge to investigate its strength. The main topic of my PhD thesis is how I successfully utilized this new method of generating pH gradient for synthesizing the first example of ultrathin membranes of artificial lignin (Figure 1). Moreover, I demonstrated its application for a separation membrane. In addition, at the early stage of the investigation of ultrathin membrane synthesis, I found an anomalously slow hydration kinetics of a self-assembled monolayer on hydrophobic surfaces in water. This finding provides a new fundamental molecular insight about how protein-ligand and protein-protein interactions take place.

Figure 1. Photograph of a free-standing 58-nm thick artificial lignin membrane transferred to a wire lasso, together with its proposed chemical structure.

【2】Fabrication and Characterization of Ultrathin Membranes of Artificial Lignin

Ultrathin membranes bearing both nanometer thickness and macroscopic size, have garnered intense scientific interest because of their potential applications in selective transport, flexible electrical skin and electrochemical devices. Two important structural features are requested for these applications to have, one is mechanical/chemical robustness, and the other is homogeneous structure

without defect over a large area. It is still a big challenge to achieve these specific targets in the development of ultrathin membranes. Lignin, as a high mechanically/chemically robust polymer would be an ideal candidate material for ultrathin membrane materials, but never fabricated to a membrane due to its low processability. Here, the author developed an extremely simple technology to fabricate an lignin-mimetic ultrathin membrane with an aspect ratio of size and thickness greater than 5×10^5.

The chemical structure of the ultrathin membrane was confirmed by Fourier transform infrared spectrometry (FT-IR) and pyrolysis–gas chromatography–mass spectrometry (Pyr-GC/MS). X-ray photoelectron spectroscopy (XPS) of the membrane exhibited two peaks in O1s region assignable to C–O and C=O. This indicate that oxidation reaction of the hydroxyl group took place. The above chemical structural feature well matches with that of lignin[1].

The thickness and the surface roughness of the membrane was determined to be 57.7 ± 0.46 nm and 2.20 nm, respectively, by using atomic force microscopy (AFM) (Figure 2a-c). Furthermore, according to scanning electron microscopic (SEM) images, the membrane does not have a defeat over a large area (Figure 2d). Furthermore, transmission electron microscope (TEM) studies further confirmed the nanomembrane was defect-free and amorphous polymer (Figure e and f). These microscopic investigations clearly demonstrated the homogeneous smooth defect-free feature of the ultrathin membrane.

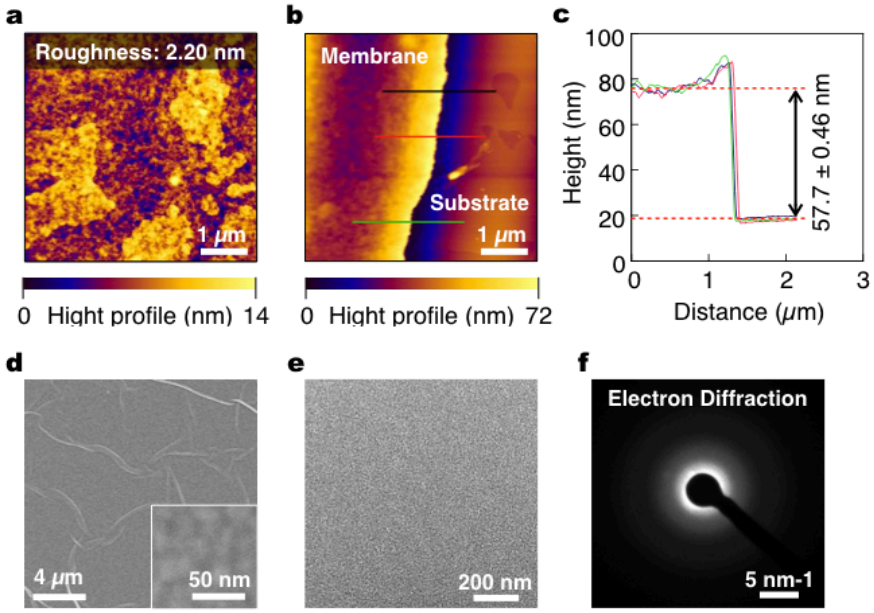

Figure 2. (**a**) AFM topography images of the membrane. (**b** and **c**) AFM height profile of the membrane. (**d**) SEM image of the membrane. (**e**) TEM images of free-standing artificial lignin nanomembrane. (**f**) Corresponding electron diffraction image.

Nanoindentation measurement confirmed that the Young's modulus of the nanomembrane is 12.5 GPa. This value is one order of magnitude higher than conventional polymeric ultrathin membranes[5]. Such mechanical robustness is likely derived from the three-dimensionally cross-linked aromatic skeleton of nanomembrane. In order to investigate chemical stability, the membrane were soaked into 0.5 M HCl and 0.5 M NaOH solution for one month. Surprisingly, AFM observation revealed that the thickness and surface morphology showed negligible change, demonstrating its excellent chemical robustness. The observed mechanical and chemical robustness is appropriate for the membranes to be utilized under strict engineering environments, such as high pressure, strong basic or acidic conditions.

Our novel technology can tailor membrane thickness down to several nanometer increments by changing the synthetic conditions. The thickness of membrane increased from 30 to 75 nm. This is likely due to the decreased diffusion rate of the monomers to the reaction surface once the membrane

became thick enough. These results clearly demonstrated that our novel technology is highly universal and has the potential to fabricate various functional ultrathin membranes.

【3】Ultrafast Water Purification Behavior of Artificial Lignin Membrane

Purification and separation using membranes are known to be an energy-efficient process and often employed in industry. Such membranes are requested to meet two requirements; one is to be robust under strict engineering environments, and the other is to have permeability for high process efficiency. Regarding the permeability, reducing the membrane thickness is the straightforward way to achieve high value, especially to a thickness below 100 nm. The ultrathin artificial lignin membrane, described in Chapter 2, was discovered to have high mechanical and chemical robustness. Considering the thickness of 58 nm, the membrane is also expected to have high permeability. In Chapter 3, water permeability and purification capability of the ultrathin artificial lignin membrane was investigated.

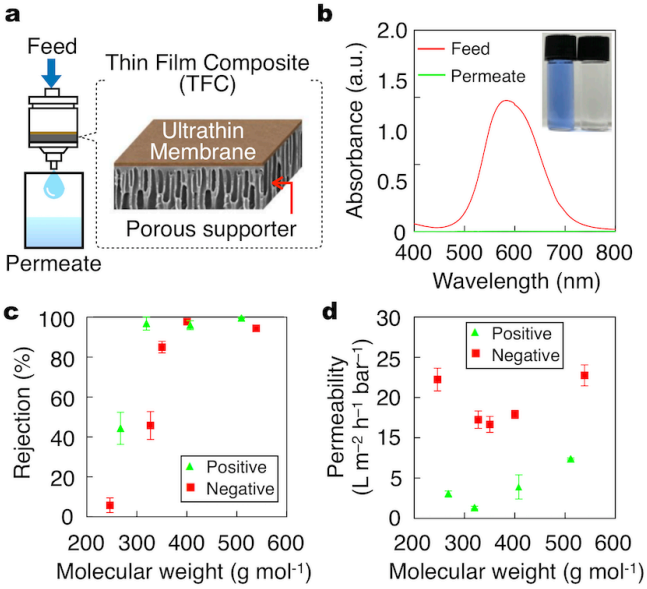

Figure 3. (**a**) Schematic representation of the dead-end filtration apparatus using thin film composite (TFC) having the ultrathin membrane on a porous support. (**b**) Electronic absorption spectra of brilliant blue G dye in water before (red trace) and after (green) the separation process using ultrathin membrane. Inset: photograph of the feed solution (left) and permeate (right). (**c**) Rejection rate versus molecular weight of various dyes. (**d**) Permeability versus molecular weight of various dyes.

The artificial lignin membrane was first placed onto a porous polymeric supporting membrane (pore size = ~100 nm) and prepared a thin film composite (TFC). The water permeation was investigated using the TFC membrane by a homemade dead-end filtration apparatus. Water has shown a high water permeability of 21.98 L m^{-2} h^{-1} bar^{-1}. This value is one order of magnitude higher than typical polyamide membrane used for water desalination. The separation performance of artificial lignin TFC membrane was also evaluated by using an aqueous solutions of various dyes. To our surprise, brilliant blue G (Mw = 854.02 g mol^{-1}) could be completely separated (rejection ratio = 99.9%) while maintaining high permeability (21.76 L m^{-2} h^{-1} bar^{-1}) (Figure 3b). Furthermore, the separation performance of artificial lignin membrane was highly dependent on the charge of the dye molecule rather than the size, which is very different compared to reported examples. As for the smaller molecules (< 350 g mol^{-1}), positively charged ones had higher rejection rate than negative ones. For example, the rejection rate of methylene blue (Mw = 319.9 g mol^{-1}, charge = +1) and methyl orange (Mw = 327.3 g mol^{-1}, charge = –1), whose molecular weight were similar but the charge were opposite, were 96.8% and 45.7%, respectively. We supposed that partial deprotonation of the hydroxy group on the polymeric

skeleton of the membrane endowed the negatively charged feature, and thus positively charged dyes can be trapped by electrostatic attractive force.

【4】 Anomalously Slow Hydration Kinetics of Self-Assembled Monolayer at Hydrophobic Interface

The hydration behaviors of polar molecules at a hydrophobic surface are long-standing interest in protein and cellular interactions. Several theoretical proposals have been made to elucidate peculiar properties of water on hydrophobic surfaces. However, before our recent work[3], this issue remained unexplored, mainly because analytical methods such as second harmonic generation (SFG) and AFM, mostly employed for investigating interfacial events, are not informative enough to render the behaviors of complex functional groups on the surface[6]. In Chapter 3, I fabricated self-assembled monolayers (SAMs) composed of polar tetraethylene glycol chains appended with nonionic (Fmoc) and ionic (FITC) fluorescent head groups on silicon wafer covered by space-filling C2 alkyl chains (SAM_{C2}) as a model and investigated their hydration events.

According to our reported methods (Figure 4), we synthesized Fmoc-SAM_{C2} and FITC-SAM_{C2}. Their area-per-molecule densities were estimated by using Fmoc-SAM_{C2}^{qtz} and FITC-SAM_{C2}^{qtz} prepared with quartz instead of silicon wafer, because their quartz substrates are optically transparent and allow for quantitative analysis of Fmoc and FITC by electronic absorption spectroscopy. The area-per-molecule densities for Fmoc-SAM_{C2}^{qtz} and FITC-SAM_{C2}^{qtz} were 2.3 and 3.1 nm^2, respectively, which are in fair agreement with each other and also close to those reported previously. In their dry state, the head groups are supposed to stay in vicinity of the silicon wafer surface. When these SAMs are dipped in water, their hydrophobic surfaces including the fluorescent head groups are immediately hydrated and embedded in a thin hydration layer (Figure 5a). Then, the TEG spacer may start to undergo a conformational change. If the TEG spacer adopts an extended conformation, the head groups are estimated to be 1.5 nm distant from the silicon wafer surface. Here, it should be noted that silicon wafer induces distance-dependent fluorescence quenching of organic dyes. Hence, we considered that the conformational changes of the TEG-appended head groups of Fmoc-SAM_{C2} and FITC-SAM_{C2} in aqueous media can be visualized by fluorescence spectroscopy.

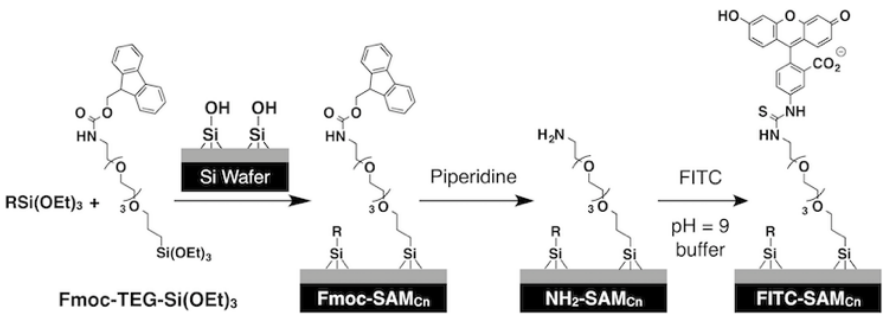

Figure 4. Synthetic procedures for Fmoc-SAM_{C2} and FITC-SAM_{C2}.

As expected, Fmoc-SAM_{C2}^{qtz} fluoresced at λ_{em} = 341 nm (λ_{ex} = 264 nm) even in its dry state. When dipped in water, Fmoc-SAM_{C2}^{qtz} showed a 14-nm blue shift in its fluorescence maximum due to the fast hydration event but did not show any subsequent fluorescence spectral change. Hence, slow fluorescence intensity change observed for Fmoc-SAM_{C2} (Figures 5) was a benefit from the distant-

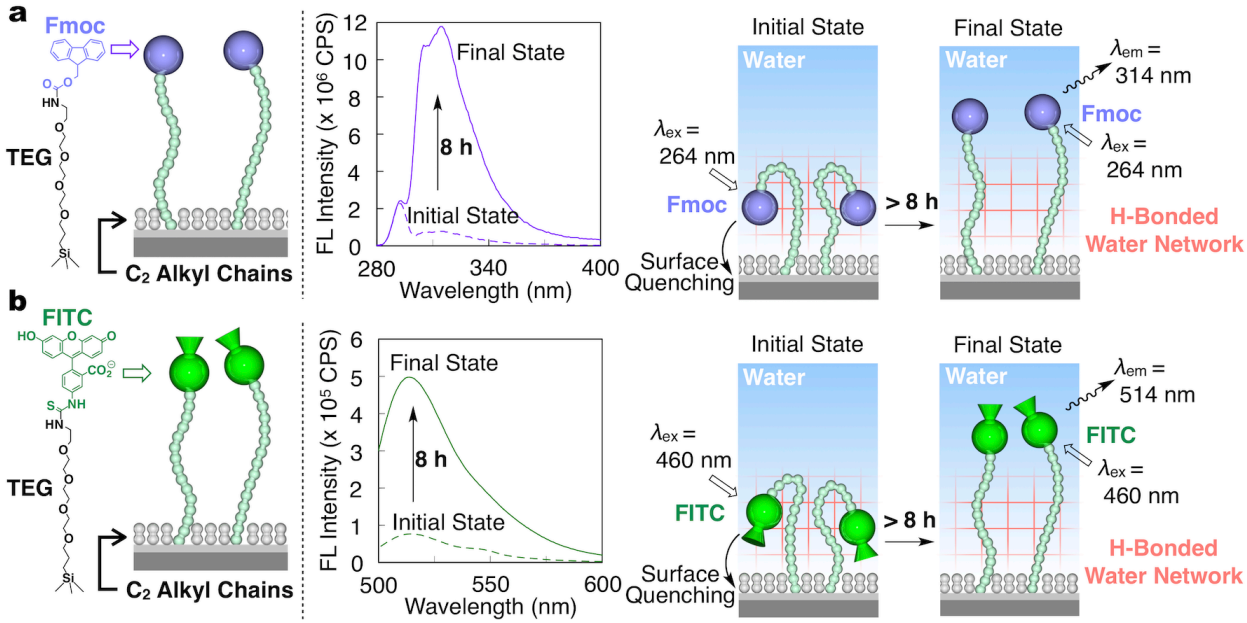

Figure 5. Molecular structures (left) and schematic representations (right) of **Fmoc-SAM$_{C2}$** (**a**) and FITC-SAM$_{C2}$ (**b**), and their fluorescence emission spectra at 25 °C (center) just after being submerged in deionized water (broken curves) followed by immersion for 8 h (solid curves). Schematic representations of the hydration process and the mechanism of fluorescence evolution process.

dependent fluorescence quenching ability of the silicon wafer substrate. These results allow us to conclude that the polar FITC head groups of Fmoc-SAM$_{C2}$ in water shows an anomalously slow conformational change. Accordingly, in situ ellipsometry showed that Fmoc-SAM$_{C2}$ gradually became thicker to reach a constant value of 0.9 nm in ~10 h (Figure 6b). Concerning that a contact angle of a water droplet on a hydrophobic surface reaches a constant value in seconds upon equilibration[7], the observed hydration kinetics are surprisingly slow. This anomalous hydration behavior is likely due to a peculiar hydrogen-bonding network known to form on hydrophobic surfaces. These results may certainly contribute to the deeper understanding of how polar functional groups on protein surfaces are hydrated and dehydrated and interact with different guest molecules.

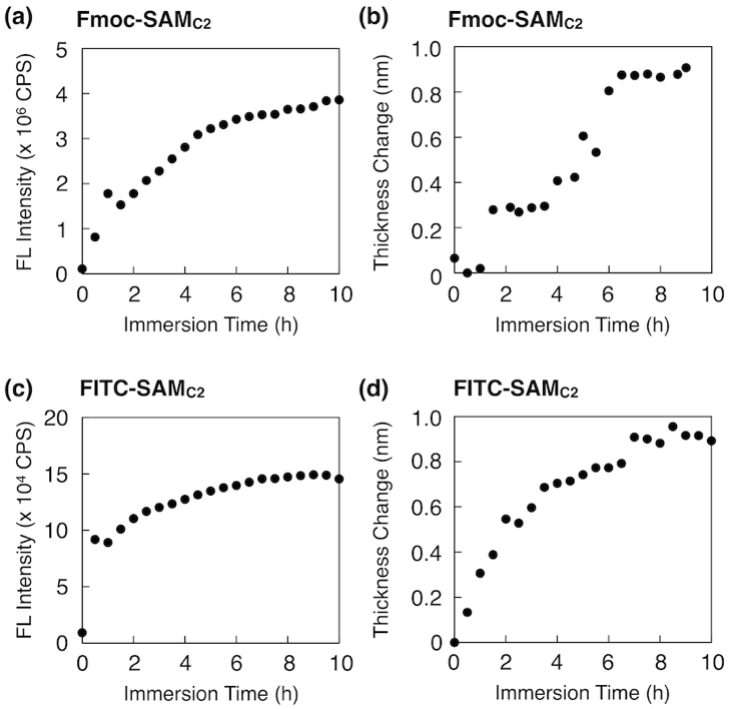

Figure 6. Time-dependent changes in (**a**, **c**) fluorescence intensity and (**b**, **d**) ellipsometric thickness of (**a**, **b**) Fmoc-SAMC2 and (**c**, **d**) FITC-SAMC2 in deionized water at 25 °C.

【5】Conclusion

In the PhD thesis, I developed a novel and universal method to fabricate an ultrathin defect-free freestanding artificial lignin membranes, which is mechanically and chemically robust, in a very simple manner. Furthermore, the composite membrane comprising artificial lignin membrane and porous supporter exhibited ultrafast water permeability, and excellent selectivity for nanofiltration applications. Considering many interesting properties of natural lignin, such as antimicrobial activity and antioxidation property, these ultrathin artificial lignin membranes might be applicable in life science. Besides, the anomalously slow hydration phenomenon at hydrophobic interface gave a clue to understand how such a hydrogen-bonded water network dominates biological functions of proteins.

【6】Publications

1. T. Fu, P.-L. Champagne, Y. Itoh, and T. Aida *to be submitted*.
2. T. Fu, X. Hao, E. Silver, S. Chen, Y. Itoh, and T. Aida, *to be submitted*.
3. T. Fu, Z. Li, Z. Zhang, X. Zhang, F. Wang, *Macromolecules*, **2017**, *50*, 7517.
4. T. Fu, L. Ao, Z. Gao, X. Zhang, F. Wang, *Chinese Chem. Lett.*, **2016**, *27*, 1147.
5. T. Fu, Y. Han, L. Ao, F. Wang, *Organometallics*, **2016**, *17*, 2850.
6. Z. Li, Y Han, Z. Gao, T. Fu, F. Wang, *Mater. Chem. Front.*, **2016**, *2*, 76.
7. T. Fu, Y. Zhang, J. Zhang, T. Wang, X. Gao, *J. Macromol. Sci. B*, **2014**, *53*, 861.

【7】References

[1] R. Vanholme R *et al*. *Plant Physiol.* **2010**, *153*, 895.
[2] V. K. Thakur *et al*. *ACS Sustain. Chem. Eng.* **2014**, *2*, 1072.
[3] S. Chen *et al*. *Science* **2015**, *348*, 555.
[4] S. Karan *et al*. *Science* **2015**, *348*, 1347.
[5] P. Gorgojo *et al*. *Adv. Funct. Mater.* **2014**, *24*, 4729.
[6] Y. Shen *et al*. *Chem. Rev.* **2006**, *106*, 1140.
[7] S. Semal *et al*. *J. Phys. Chem. B*, **2000**, *104*, 6225.